Nuclear medium effects in $\nu(\bar{\nu})$-nucleus deep inelastic scattering

H. Haider,[1] I. Ruiz Simo,[2,3] M. Sajjad Athar,[1,*] and M. J. Vicente Vacas[2]

[1]*Department of Physics, Aligarh Muslim University, Aligarh-202 002, India*

[2]*Departamento de Física Teórica and IFIC, Centro Mixto Universidad de Valencia-CSIC, Institutos de Investigación de Paterna, E-46071 Valencia, Spain*

[3]*Departamento de Física Atómica Molecular y Nuclear, Universidad de Granada, E-18071 Granada, Spain*

(Received 17 August 2011; published 15 November 2011)

We study nuclear medium effects in the weak structure functions $F_2(x, Q^2)$ and $F_3(x, Q^2)$ in the deep inelastic neutrino and antineutrino induced reactions in nuclei. We use a theoretical model for the nuclear spectral functions which incorporates the conventional nuclear effects, such as Fermi motion, binding, and nucleon correlations. We also consider the pion and rho meson cloud contributions calculated from a microscopic model for meson-nucleus self-energies. The calculations have been performed using relativistic nuclear spectral functions. Our results are compared with the experimental data of the NuTeV and the CERN Dortmund Heidelberg Saclay Warsaw (CDHSW) collaborations.

DOI: 10.1103/PhysRevC.84.054610 PACS number(s): 13.15.+g, 24.10.−i, 24.85.+p, 25.30.Pt

I. INTRODUCTION

Nuclear-medium effects in deep inelastic scattering processes have been widely discussed after the measurement and comparison of the iron and deuterium electromagnetic structure functions $F_2^N(x, Q^2)$ by the European Muon Collaboration at CERN using charged lepton beams [1]. Thereafter, both theoretical as well as experimental studies have been made of several nuclei. Presently, most of the information on nuclear-medium effects comes from the charged lepton scattering data. The weak structure functions $F_2^N(x, Q^2)$ and $F_3^N(x, Q^2)$ have also been measured using neutrino (antineutrino) beams [2–9]. More experiments are planned to obtain data in the deep inelastic region using neutrino and antineutrino beams that will complement the information obtained from the charged lepton scattering. The nuclear effects for the weak structure functions $F_2^A(x, Q^2)$ and $F_3^A(x, Q^2)$ may, in general, be different. Moreover, the nuclear correction for the weak structure function $F_2^A(x, Q^2)$ may be different from the correction for the electromagnetic structure function $F_2^{EM,A}(x, Q^2)$. The precise measurement of the deep inelastic scattering $\nu(\bar{\nu})$ cross section is also important in providing global fits of the parton distribution functions (PDFs) and, due to the fact that most of the $\nu(\bar{\nu})$ experiments are being performed with nuclear targets, the nuclear effects should be properly accounted for before extracting the free nucleon parton distribution function. In the determination of electroweak parameters, a good knowledge of the nuclear medium effect is required.

Furthermore, with the confirmation of the neutrino oscillation hypothesis in the atmospheric as well as accelerator-based experiments, the target is to precisely determine the parameters of the neutrino mass mixing matrix (PMNS matrix), particularly to get some information on mixing angle θ_{13} and the CP-violating phase δ, using long-baseline neutrino experiments and getting neutrinos from factories as well as β-beam sources [10]. Most of these experiments are in the few-GeV-energy region. These high-intensity neutrino sources are aimed to reduce statistical uncertainties. Recently, more efforts have been made to understand the systematic uncertainties [11]. This is because, in the region of a few GeV which is sensitive to the determination of the parameters of PMNS matrix, the cross sections have not been very well measured. Due to this reason, various experiments are being done or have been proposed and lots of theoretical studies have been made recently for understanding nuclear-medium effects. These theoretical studies are mainly done for the quasielastic and one-pion production processes, and recently some work on the two-pion production, nucleon knockout reaction, hyperon production, and single-kaon production has been performed. In the case of the deep inelastic scattering process induced by the weak interaction, there are very few calculations where the dynamical origin of the nuclear-medium effects has been studied [12,13]. In some theoretical analyses, nuclear-medium effects have been phenomenologically described in terms of a few parameters which are determined from fitting the experimental data of charged lepton and (anti)neutrino deep inelastic scattering from various nuclear targets [14–21].

The MINERνA Collaboration [22] is taking data using neutrinos from the NuMI Laboratory, and their aim is to perform cross-section measurements in the neutrino-energy region of 1 to 20 GeV and with various nuclear targets like carbon, iron, and lead. This will experimentally complement the present theoretical understanding of nuclear-medium effects. The neutrino scattering on glass (NuSOnG) experiment [23,24] has been proposed at Fermilab to study the structure functions in the deep inelastic region using neutrino sources. The NuTeV Collaboration [9] has reported results of weak-charged- and neutral-current-induced (anti)neutrino processes with an iron target in the deep inelastic region. The Neutrino Oscillation Magnetic Detector (NOMAD) Collaboration [25] is doing data analysis of their experimental results and is very soon going to report the results for the structure functions and cross sections in a carbon target using a neutrino beam.

*sajathar@gmail.com

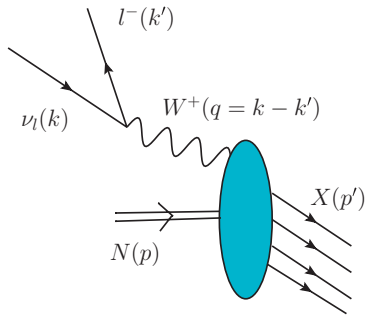

FIG. 1. (Color online) Feynman diagram for the deep inelastic ν-nucleon scattering.

In this paper, we study nuclear-medium effects on the structure functions $F_2(x,Q^2)$ and $F_3(x,Q^2)$ in iron and carbon nuclear targets. We use a relativistic nucleon spectral function [26] to describe the momentum distribution of nucleons in the nucleus and define everything within a field-theoretical approach where nucleon propagators are written in terms of this spectral function. The spectral function has been calculated using Lehmann's representation for the relativistic nucleon propagator and nuclear many-body theory is used to calculate it for an interacting Fermi sea in nuclear matter. A local-density approximation is then applied to translate these results to finite nuclei [13,27,28]. We have assumed the Callan-Gross relationship for nuclear structure functions $F_2{}^A(x)$ and $F_1{}^A(x)$. The contributions of the pion and rho meson clouds are taken into account in a many-body field-theoretical approach which is based on Refs. [27,29]. We have taken into account target mass correction (TMC) following Ref. [30], which has significant effect at low Q^2, moderate and high Bjorken x. To take into account the shadowing effect, which is important at low Q^2 and low x and which modulates the contribution of pion and rho cloud contributions, we have followed the works of Kulagin and Petti [12,31]. Since we have also applied the present formalism at low Q^2, we have not assumed the Bjorken limit. Recently, we have applied the present formalism to study nuclear effects in the electromagnetic structure function $F_2(x, Q^2)$ in nuclei in deep inelastic lepton nucleus scattering [28] and found that the numerical results agree with recent results from the Thomas Jefferson National Accelerator Facility (JLab), where the data for the ratios $R^A_{F2}(x, Q^2) = [2F_2^A(x, Q^2)]/[AF_2^{\text{Deuteron}}(x, Q^2)]$ have been obtained [32], and also with some of the earlier experiments performed using heavier nuclear targets. Motivated by the success of the present formalism [13,27,28,33], we have studied in this paper the nuclear-medium effects in the weak structure functions $F_2(x,Q^2)$ and $F_3(x,Q^2)$ and have compared our results with the experimental results of NuTeV and CDHSW. Furthermore, we have obtained the ratio of the structure functions $R^A_{F_i}(x, Q^2) = [2F_i^A(x, Q^2)]/[AF_i^{\text{Deuteron}}(x, Q^2)]$ $(i = 2, 3)$ to see how they compare with the ratio obtained earlier for the electromagnetic structure function. Using these $F_2(x,Q^2)$ and $F_3(x,Q^2)$ structure functions, we have obtained the differential scattering cross sections in iron and carbon nuclear targets. The results in iron are compared with the available experimental data and the results in carbon would be a good test of our model when NOMAD [25] results come up.

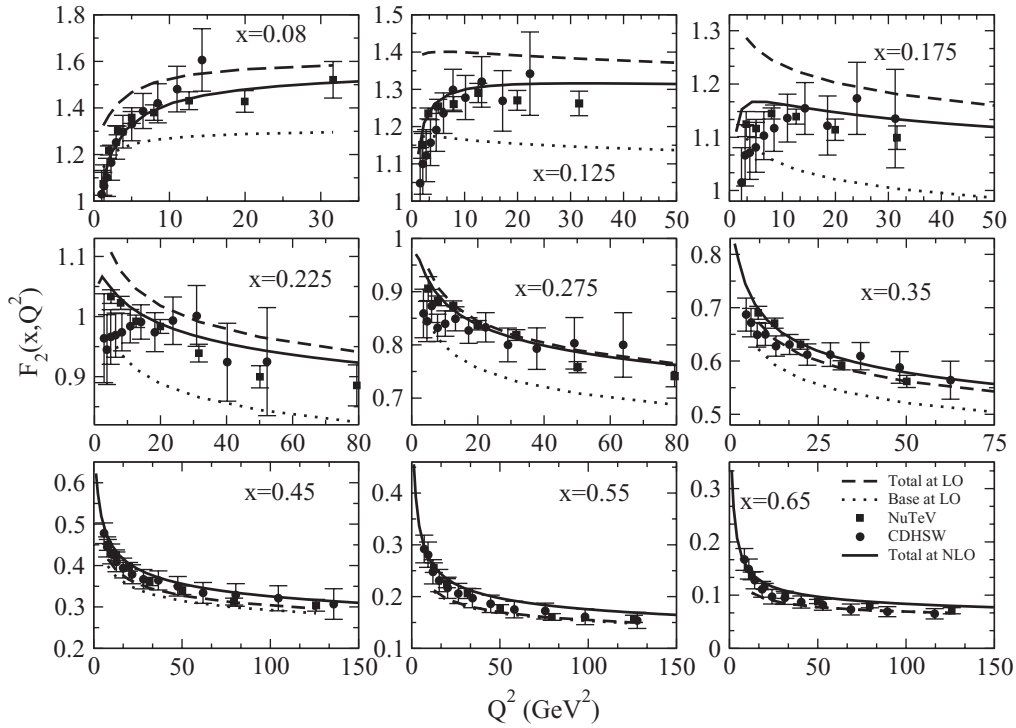

FIG. 2. Dotted line is $F_2(x, Q^2)$ vs Q^2 in ^{56}Fe calculated using Eq. (13) with TMC. For the calculations, CTEQ [35] PDFs at LO have been used. Dashed line is the full model at LO. Solid line is full calculation at NLO. The experimental points are from CDHSW [3] (solid circles) and NuTeV [9] (solid squares).

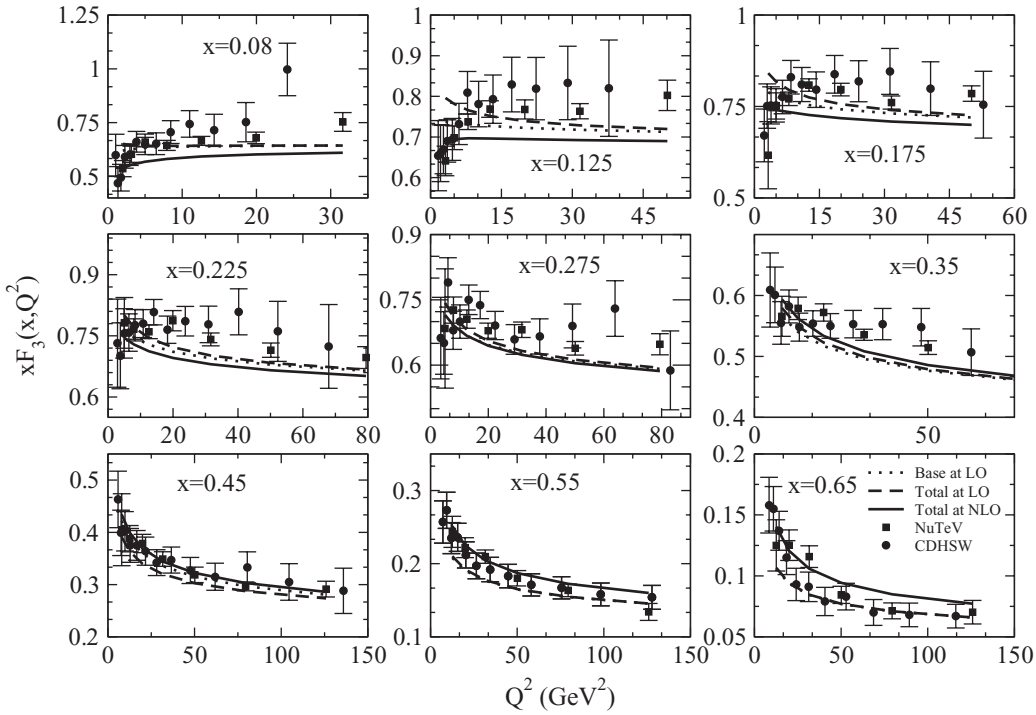

FIG. 3. $xF_3(x, Q^2)$ vs Q^2 in ^{56}Fe. Lines and points have the same meaning as in Fig. 2.

The plan of the paper is as follows: In Sec. II we introduce some basic formalism for lepton-nucleon scattering, in Sec. III we analyze the different nuclear effects, and in Sec. IV we present the results of our calculations and compare them with the available experimental results. In Sec. V we conclude our findings.

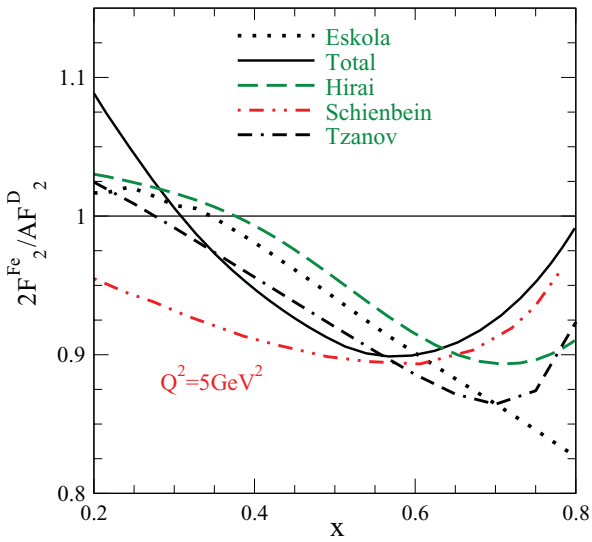

FIG. 4. (Color online) Ratio $R(x, Q^2) = \frac{2F_2^{\rm Fe}}{AF_2^{\rm D}}$ with full calculation has been shown by the solid line. Calculations have been done for $Q^2 = 5$ GeV^2 using CTEQ [35] PDFs at NLO. The results from Tzanov *et al.* [9] (double-dash dotted line), Hirai *et al.* [15] (dashed line), Eskola *et al.* [18] (dotted line), and Schienbein *et al.* [21] (double-dot dashed line) have also been shown.

II. FORMALISM

The expression of the differential cross section for deep inelastic scattering (DIS) of neutrinos with a nucleon target induced by charged current reaction

$$\nu_l(k) + N(p) \to l^-(k') + X(p'), \quad l = e, \mu, \tag{1}$$

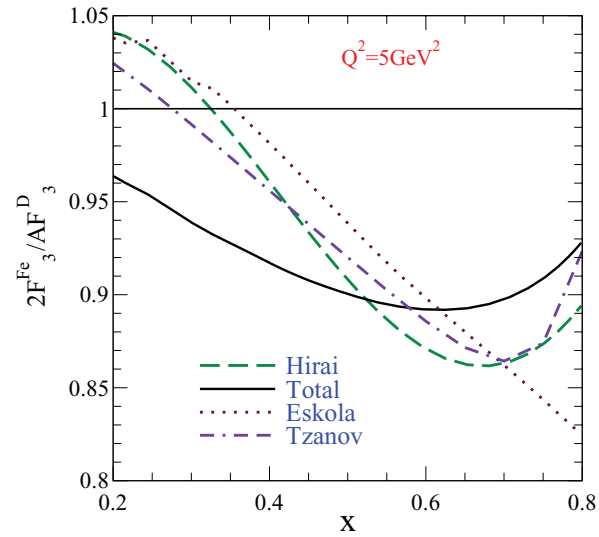

FIG. 5. (Color online) Ratio $R(x, Q^2) = \frac{2F_3^{\rm Fe}}{AF_3^{\rm D}}$ with full calculation shown by solid line. Calculations have been done for $Q^2 = 5$ GeV^2 using CTEQ [35] PDFs at NLO. The results from Tzanov *et al.* [9] (double-dash dotted line), Hirai *et al.* [15] (dashed line), and Eskola *et al.* [18] (dotted line) are also shown.

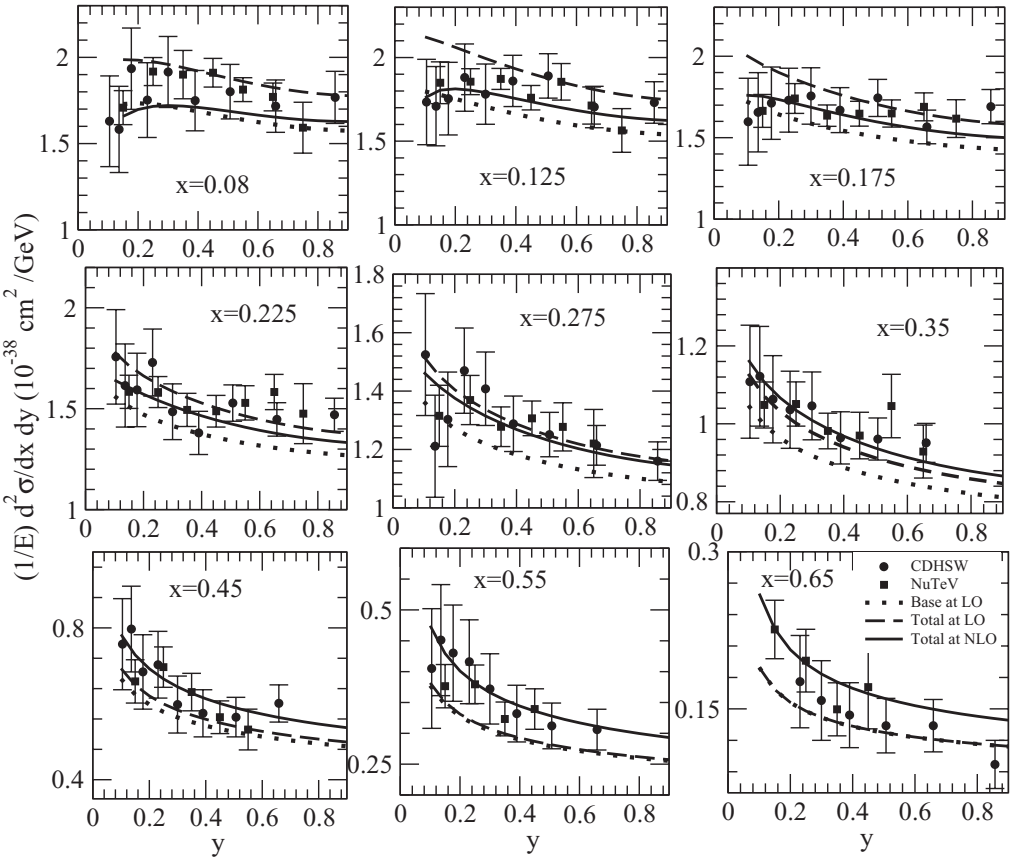

FIG. 6. $\frac{1}{E}\frac{d^2\sigma}{dxdy}$ vs y at different x for ν_μ-induced ($E_{\nu_\mu} = 65$ GeV) reaction in ^{56}Fe. Lines and points have the same meaning as in Fig. 2.

shown in Fig. 1, is given in terms of the Bjorken variables x and y and the dimensionless structure functions F_i ($i = 1$ to 5) by

$$\frac{d^2\sigma^{\nu(\bar{\nu})}}{dxdy} = \frac{G_F^2 M E_\nu}{\pi\left(1+Q^2/M_W^2\right)^2}\left\{\left(y^2x + \frac{m_l^2 y}{2E_\nu M}\right)F_1(x,Q^2) + \left[\left(1-\frac{m_l^2}{4E_\nu^2}\right) - \left(1+\frac{Mx}{2E_\nu}\right)y\right]F_2(x,Q^2) \pm\left[xy\left(1-\frac{y}{2}\right) - \frac{m_l^2 y}{4E_\nu M}\right]F_3(x,Q^2) + \frac{m_l^2(m_l^2+Q^2)}{4E_\nu^2 M^2 x}F_4(x,Q^2) - \frac{m_l^2}{E_\nu M}F_5(x,Q^2)\right\}, \quad (2)$$

where G_F is the Fermi coupling constant, m_l is the mass of lepton, E_ν is the incident neutrino or antineutrino energy, and M is the mass of nucleon. In F_3 the + (−) sign is for neutrino (antineutrino), $x(=\frac{Q^2}{2M\nu})$ is the Bjorken variable, $y = \frac{\nu}{E_\nu}$, ν and q are the energy and momentum transfer of leptons respectively, and $Q^2 = -q^2$. F_4 and F_5 are generally omitted since they are suppressed by a factor of at least $m_l^2/(2ME_\nu)$ relative to the contributions of F_1, F_2, and F_3. F_1 and F_2 are related by the Callan-Gross relation [34] leading to only two independent structure functions F_2 and F_3. The nucleon structure functions are determined in terms of parton distribution functions for quarks and antiquarks. For the numerical calculations, parton distribution functions for the nucleons have been taken from the parametrization of the Coordinated Theoretical-Experimental Project on QCD (CTEQ) Collaboration (CTEQ6.6) [35]. The Next-to-Leading-Order (NLO) evolution of the deep inelastic structure functions has been taken from the works of Moch *et al*. [36–38].

III. NUCLEAR EFFECTS IN NEUTRINO SCATTERING

When the reaction given by Eq. (1) takes place in a nucleus, several nuclear effects have to be considered. In general one may categorize these medium effects into two parts: a kinematic effect which arises because the struck nucleon is not at rest but is moving with a Fermi momentum in the rest frame of the nucleus, and a dynamic effect which arises due to the strong interaction of the initial nucleon in the nuclear medium.

In a nuclear medium the expression for the cross section is written as

$$\frac{d^2\sigma^A_{\nu,\bar{\nu}}}{d\Omega' dE'} = \frac{G_F^2}{(2\pi)^2}\frac{|\mathbf{k}'|}{|\mathbf{k}|}\left(\frac{m_W^2}{q^2-m_W^2}\right)^2 L^{\alpha\beta}_{\nu,\bar{\nu}} W^A_{\alpha\beta}, \quad (3)$$

where $W^A_{\alpha\beta}$ is the nuclear hadronic tensor defined in terms of nuclear hadronic structure functions $W^A_i(x, Q^2)$:

$$W^A_{\alpha\beta} = \left(\frac{q_\alpha q_\beta}{q^2} - g_{\alpha\beta}\right) W^A_1 + \frac{1}{M_A^2}\left(p_\alpha - \frac{p\cdot q}{q^2} q_\alpha\right) \times \left(p_\beta - \frac{p\cdot q}{q^2} q_\beta\right) W^A_2 - \frac{i}{2M_A^2}\epsilon_{\alpha\beta\rho\sigma} p^\rho q^\sigma W^A_3, \quad (4)$$

where M_A is the mass of the nucleus. $L^{\alpha\beta}$ is the leptonic tensor given by

$$L^{\alpha\beta} = k^\alpha k'^\beta + k^\beta k'^\alpha - k.k' g^{\alpha\beta} \pm i\epsilon^{\alpha\beta\rho\sigma} k_\rho k'_\sigma, \quad (5)$$

with the $-$ sign for neutrino and the $+$ sign for antineutrino in the antisymmetric term.

$W^A_i(x, Q^2)$ are redefined in terms of the dimensionless structure functions $F^A_i(x, Q^2)$ through

$$\begin{aligned} M_A W^A_1(\nu, Q^2) &= F^A_1(x, Q^2), \\ \nu W^A_2(\nu, Q^2) &= F^A_2(x, Q^2), \\ \nu W^A_3(\nu, Q^2) &= F^A_3(x, Q^2). \end{aligned} \quad (6)$$

In the local-density approximation the reaction takes place at a point $\mathbf{r}$, lying inside the nuclear volume element d^3r with local density $\rho_p(\mathbf{r})$ and $\rho_n(\mathbf{r})$ corresponding to the proton and neutron densities, respectively, and the neutrino nuclear cross sections are obtained in terms of the neutrino self-energy $\Sigma(k)$ in the nuclear medium:

$$\Sigma(k) = (-i)\frac{G_F}{\sqrt{2}}\frac{4}{m_\nu}\int \frac{d^4k'}{(2\pi)^4}\frac{1}{k'^2 - m_l^2 + i\epsilon} \times \left(\frac{m_W}{q^2 - m_W^2}\right)^2 L_{\alpha\beta}\Pi^{\alpha\beta}(q), \quad (7)$$

where $\Pi^{\alpha\beta}(q)$ is the W self-energy in the nuclear medium [27]:

$$\begin{aligned} -i\Pi^{\alpha\beta}(q) = (-)\int \frac{d^4p}{(2\pi)^4} iG(p) \sum_X \sum_{s_p, s_i} \prod_{i=1}^{n} \int \frac{d^4p'_i}{(2\pi)^4} \\ \times \prod_l iG_l(p'_l) \prod_j iD_j(p'_j) \left(\frac{-G_F m_W^2}{\sqrt{2}}\right) \\ \times \langle X|J^\alpha|N\rangle \langle X|J^\beta|N\rangle^* (2\pi)^4 \delta^4 \\ \times \left(q + p - \Sigma_{i=1}^n p'_i\right). \end{aligned} \quad (8)$$

X is the final state, which consists of fermions and bosons. l and j are indices for the fermions and bosons, respectively. $G_l(p'_l)$ and $D_j(p'_j)$ are respectively the nucleon and meson relativistic propagators in the final state [39]. $G(p)$ is the nucleon propagator with mass M and energy $E(\mathbf{p})$ in the initial state, which is calculated for a relativistic nucleon in the interacting Fermi sea by making a perturbative expansion of $G(p)$ in terms of $G^0(p)$, the free nucleon propagator, and

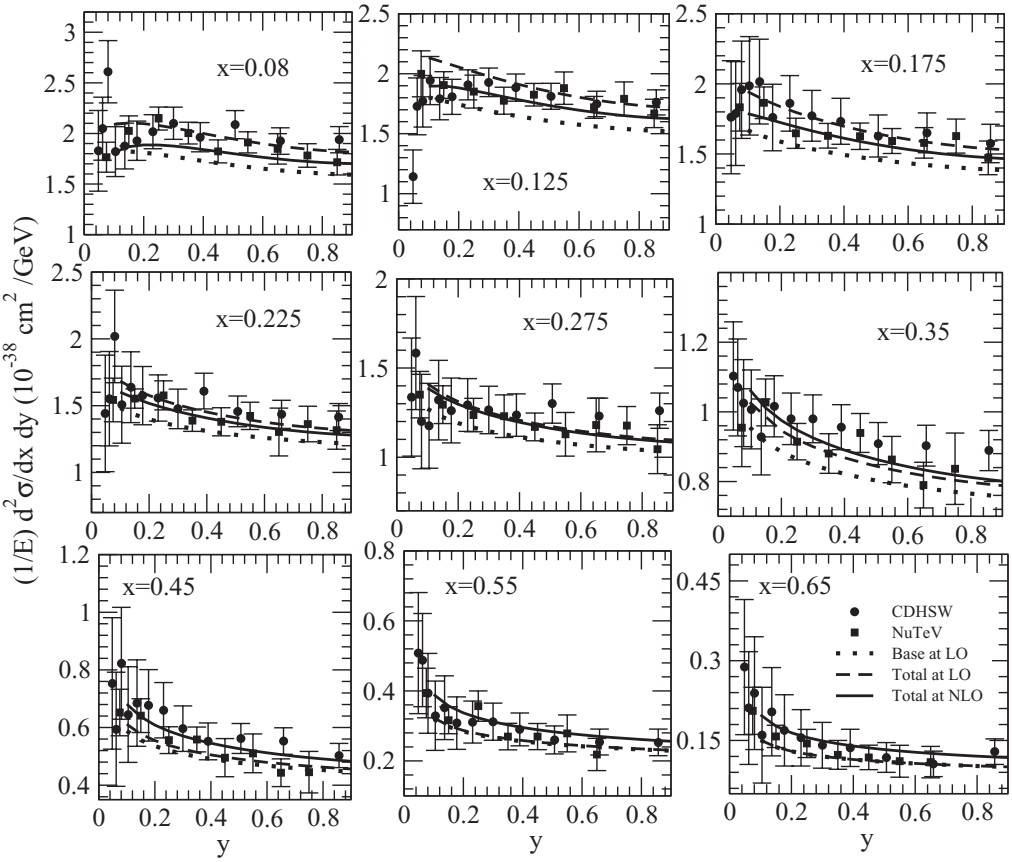

FIG. 7. $\frac{1}{E}\frac{d^2\sigma}{dxdy}$ vs y at different x for ν_μ-induced ($E_{\nu_\mu} = 150$ GeV) reaction in ^{56}Fe. Lines and points have the same meaning as in Fig. 2.

applying the ladder approximation to give [27]

$$G(p) = \frac{M}{E(\mathbf{p})} \sum_r \frac{u_r(\mathbf{p})\bar{u}_r(\mathbf{p})}{p^0 - E(\mathbf{p}) - \bar{u}_r(\mathbf{p}) \sum^N (p^0, \mathbf{p}) u_r(\mathbf{p}) \frac{M}{E(\mathbf{p})}}, \tag{9}$$

where $u_r(\mathbf{p})$ is the Dirac spinor with the normalization $\bar{u}_r(\mathbf{p})u_r(\mathbf{p}) = 1$ and $\Sigma^N(p^0, p)$ is the nucleon self-energy in nuclear matter taken from Ref. [26].

The relativistic nucleon propagator $G(p)$ in a nuclear medium is then expressed as [27]

$$G(p) = \frac{M}{E(\mathbf{p})} \sum_r u_r(\mathbf{p})\bar{u}_r(\mathbf{p}) \left[\int_{-\infty}^{\mu} d\omega \frac{S_h(\omega, \mathbf{p})}{p^0 - \omega - i\eta} + \int_{\mu}^{\infty} d\omega \frac{S_p(\omega, \mathbf{p})}{p^0 - \omega + i\eta} \right], \tag{10}$$

where $S_h(\omega, \mathbf{p})$ and $S_p(\omega, \mathbf{p})$ are the hole and particle spectral functions, respectively, μ is the chemical potential and, for the present numerical calculations, have been taken from Ref. [26]. We ensure that the spectral function is properly normalized and we get the correct Baryon number and binding energy for the nucleus.

The cross section for neutrino scattering from an element of volume d^3r in the nucleus is given by [13]

$$d\sigma = -\frac{2m_\nu}{|\mathbf{k}|} \mathrm{Im}\Sigma d^3r. \tag{11}$$

Using Eq. (7) in Eq. (11) and using Eq. (3), we get the expression for the differential scattering cross section in the local-density approximation with the hadronic tensor $W^A_{\alpha\beta}$

$$W^A_{\alpha\beta} = 4 \int d^3r \int \frac{d^3p}{(2\pi)^3} \int_{-\infty}^{\mu} dp^0 \frac{M}{E(\mathbf{p})} S_h \times (p^0, \mathbf{p}, \rho(r)) W^N_{\alpha\beta}(p, q), \tag{12}$$

where $W^N_{\alpha\beta}(p, q)$ is the hadronic tensor for the free nucleon target that is given by Eq. (4) with M_A replaced by the nucleon mass M.

Using Eqs. (3), (4), (6), and (12), we get the following expressions for $F^A_2(x)$ and $F^A_3(x)$ [13]:

$$F^A_2(x_A, Q^2) = 4 \int d^3r \int \frac{d^3p}{(2\pi)^3} \frac{M}{E(\mathbf{p})} \int_{-\infty}^{\mu} dp^0 S_h \times (p^0, \mathbf{p}, \rho(\mathbf{r})) \frac{x}{x_N} \left(1 + \frac{2x_N p_x^2}{M\nu_N}\right) F^N_2(x_N, Q^2), \tag{13}$$

$$F^A_3(x_A, Q^2) = 4 \int d^3r \int \frac{d^3p}{(2\pi)^3} \frac{M}{E(\mathbf{p})} \int_{-\infty}^{\mu} dp^0 S_h \times (p^0, \mathbf{p}, \rho(\mathbf{r})) \frac{p^0\gamma - p_z}{(p^0 - p_z\gamma)\gamma} F^N_3(x_N, Q^2), \tag{14}$$

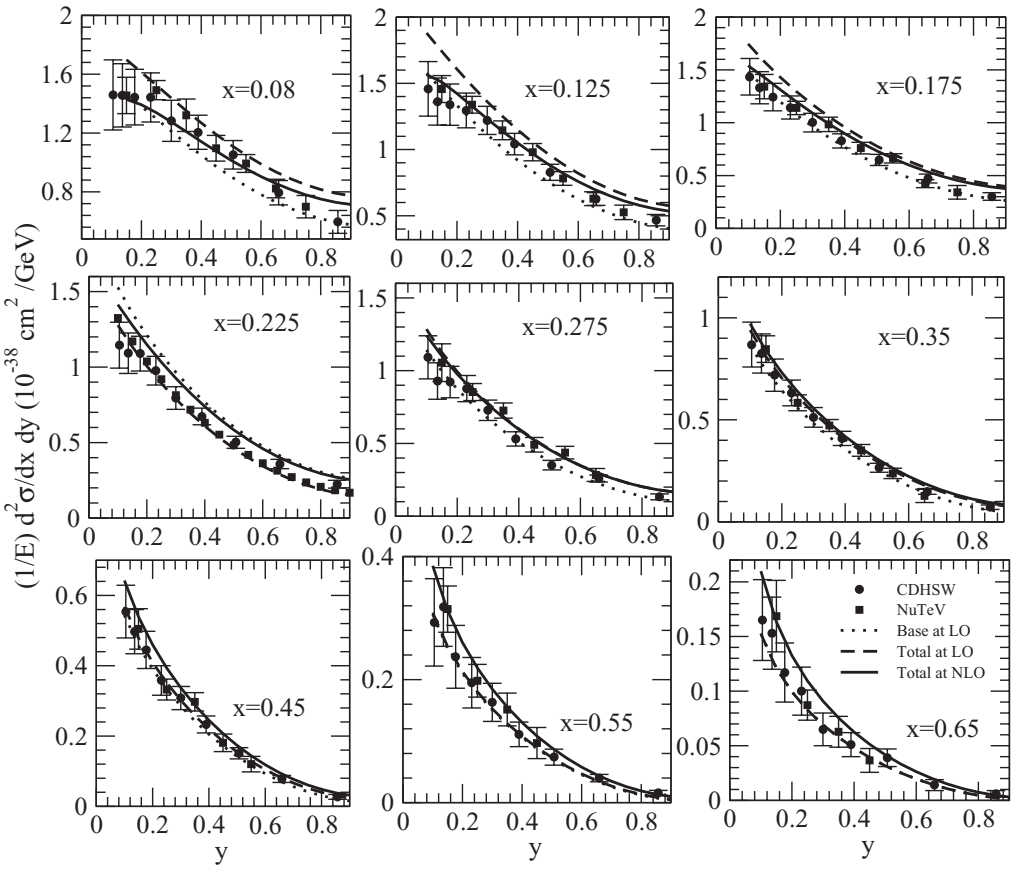

FIG. 8. $\frac{1}{E}\frac{d^2\sigma}{dxdy}$ vs y at different x for $\bar{\nu}_\mu$-induced ($E_{\bar{\nu}_\mu} = 65$ GeV) reaction in ^{56}Fe. Lines and points have the same meaning as in Fig. 2.

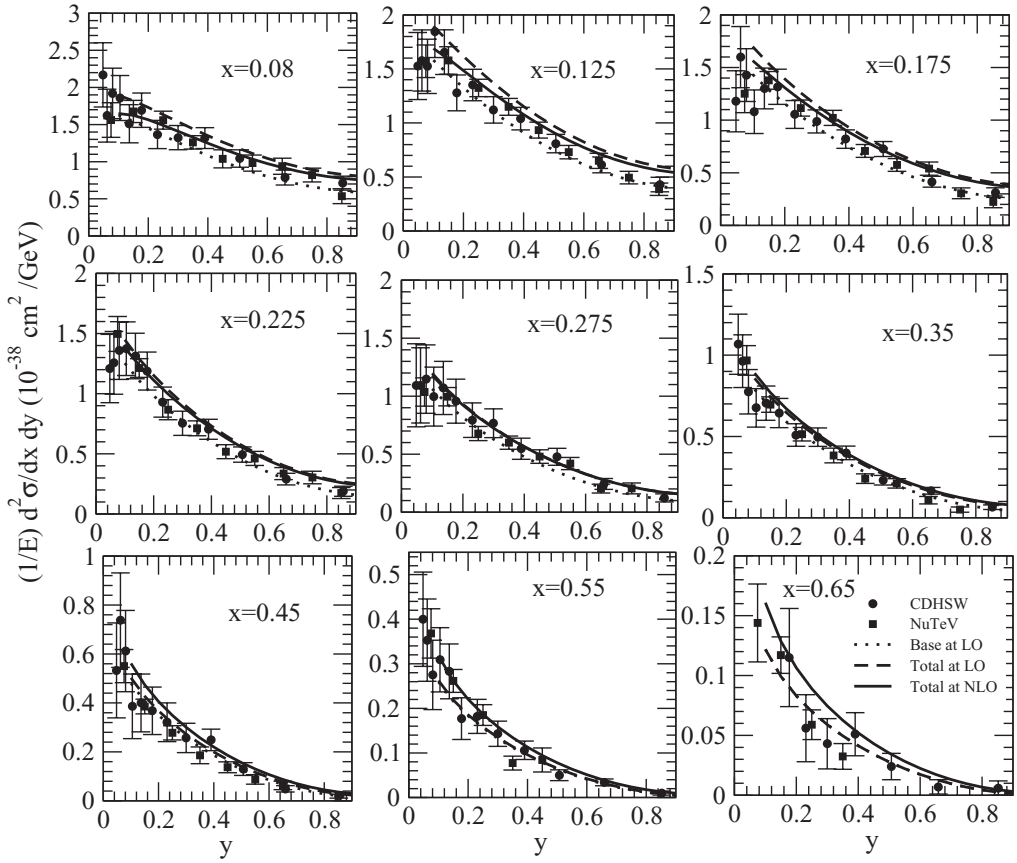

FIG. 9. $\frac{1}{E}\frac{d^2\sigma}{dxdy}$ vs y at different x for $\bar{\nu}_\mu$-induced ($E_{\bar{\nu}_\mu} = 150$ GeV) reaction in ^{56}Fe. Lines and points have the same meaning as in Fig. 2.

where

$$\gamma = \frac{q_z}{q^0} = \left(1 + \frac{4M^2x^2}{Q^2}\right)^{1/2}, \tag{15}$$

and

$$x_N = \frac{Q^2}{2(p^0q^0 - p_zq_z)}.$$

A. π and ρ meson contribution to nuclear structure function

The pion and rho meson cloud contributions to the F_2 structure function have been implemented following the many-body field-theoretical approach of Refs. [27,29]. We have performed the numerical calculations for isoscalar nuclear targets as the experimental results reported by the CDHSW [3] and NuTeV [9] collaborations are corrected for the nonisoscalarity in the iron target. In the case of the F_3 structure function there are no contributions from the pion and rho meson clouds because it only gets contributions from valence quark distributions $[(u - \bar{u}) + (d - \bar{d})]$.

The pion structure function $F_{2A,\pi}(x)$ is written as [27]

$$F^A_{2,\pi}(x) = -6\int d^3r \int \frac{d^4p}{(2\pi)^4}\theta(p^0)\delta Im D(p)\frac{x}{x_\pi} \times 2MF_{2\pi}(x_\pi)\theta(x_\pi - x)\theta(1 - x_\pi), \tag{16}$$

where $D(p)$ is the pion propagator in the nuclear medium which is given in terms of the pion self-energy Π_π:

$$D(p) = \left[p_0^2 - \vec{p}^2 - m_\pi^2 - \Pi_\pi(p^0, p)\right]^{-1}, \tag{17}$$

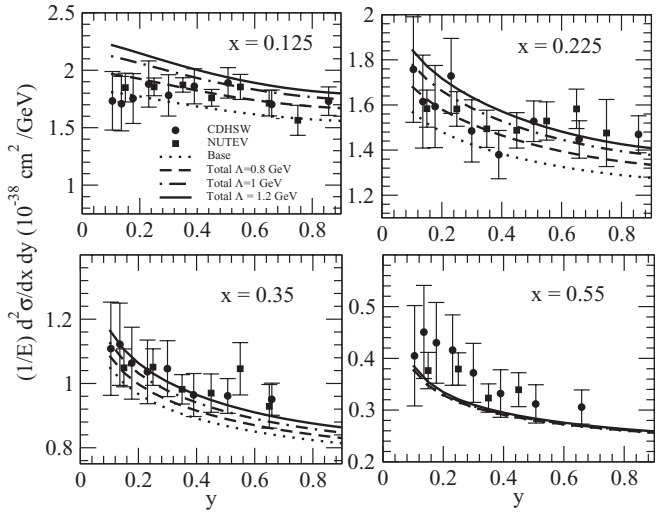

FIG. 10. $\frac{1}{E}\frac{d^2\sigma}{dxdy}$ vs y at different x for ν_μ-induced reaction in ^{56}Fe at $E_{\nu_\mu} = 65$ GeV using CTEQ [35] PDF at LO. Full model with Λ, $\Lambda_\rho = 0.8$ GeV (dashed line), Λ, $\Lambda_\rho = 1$ GeV (dash-dotted line), and Λ, $\Lambda_\rho = 1.2$ GeV (solid line). Full model without pion, rho, and shadowing is shown by dotted line. NuTeV [9] data are shown by the squares and CDHSW [3] data by the circles.

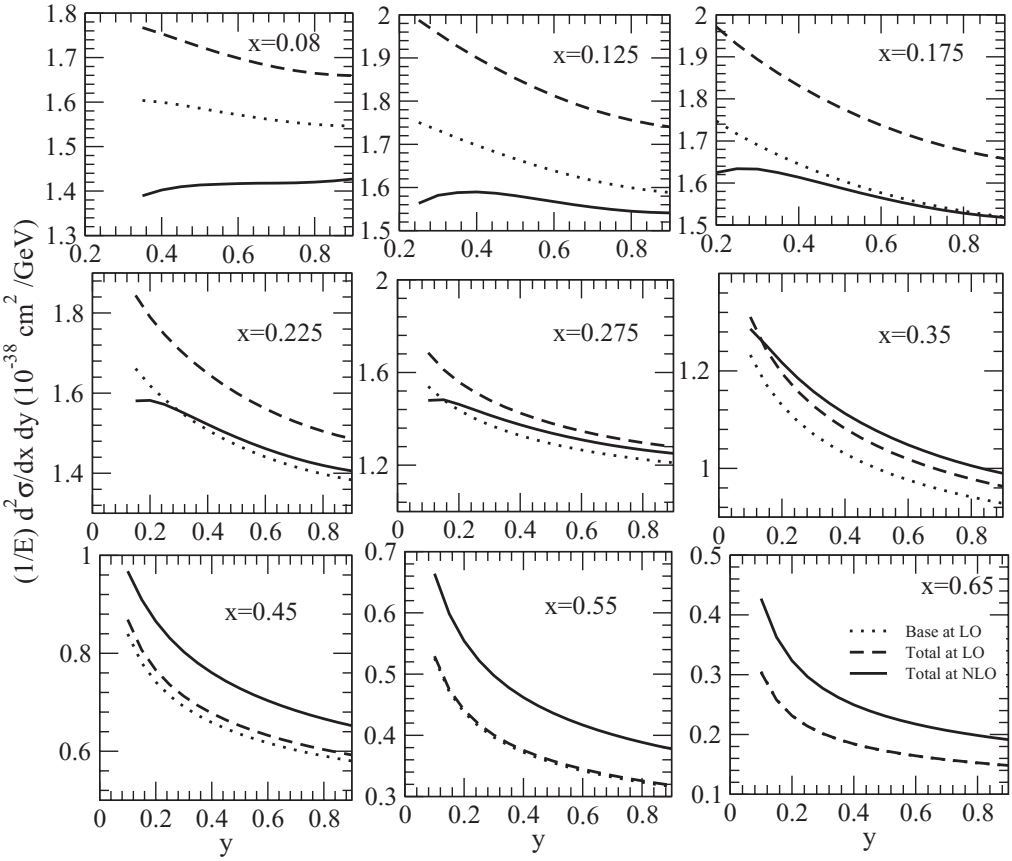

FIG. 11. $\frac{1}{E}\frac{d^2\sigma}{dxdy}$ vs y at different x for ν_μ-induced ($E_{\nu_\mu} = 20$ GeV) reaction in ^{12}C. Lines have the same meaning as in Fig. 2.

where

$$\Pi_\pi = \frac{\left[f^2/m_\pi^2\right]F^2(p)\vec{p}^{\,2}\Pi^*}{1-\left[f^2/m_\pi^2\right]V_L'\Pi^*}. \tag{18}$$

Here, $F(p) = (\Lambda^2 - m_\pi^2)/(\Lambda^2 + \vec{p}^{\,2})$ is the πNN form factor and $\Lambda = 1$ GeV, $f = 1.01$, V_L' is the longitudinal part of the spin-isospin nucleon-nucleon interaction, and Π^* is the irreducible pion self-energy that contains the contribution of particle-hole and delta-hole excitations. In Eq. (16), $\delta ImD(p)$ is given by

$$\delta ImD(p) \equiv ImD(p) - \rho\left.\frac{\partial ImD(p)}{\partial\rho}\right|_{\rho=0} \tag{19}$$

and

$$\frac{x}{x_\pi} = \frac{-p^0 + p^z}{M}. \tag{20}$$

Assuming SU(3) symmetry and following the same notation as in Ref. [40], the pion structure function at the Leading-Order (LO) can be written in terms of pionic PDFs as

$$F_{2\pi}(x_\pi) = x_\pi[2v_\pi(x_\pi) + 6\bar{q}_\pi(x_\pi)], \tag{21}$$

where $v_\pi(x_\pi)$ is the valence distribution and $\bar{q}_\pi(x_\pi)$ is the light SU(3)-symmetric sea distribution.

Similarly, the contribution of the ρ-meson cloud to the structure function is written as [27]

$$F_{2,\rho}^A(x) = -12\int d^3r\int\frac{d^4p}{(2\pi)^4}\theta(p^0)\delta ImD_\rho(p)\frac{x}{x_\rho} \times 2MF_{2\rho}(x_\rho)\theta(x_\rho - x)\theta(1-x_\rho), \tag{22}$$

where $D_\rho(p)$ is the ρ meson propagator and $F_{2\rho}(x_\rho)$ is the ρ meson structure function, which we have taken as equal to the pion structure function $F_{2\pi}$ using the valence and sea pionic PDFs from Ref. [40]. Λ_ρ in the ρNN form factor $F(p) = (\Lambda_\rho^2 - m_\rho^2)/(\Lambda_\rho^2 + \vec{p}^{\,2})$ has also been taken as 1 GeV. In the case of pions we have taken the pionic parton distribution functions given by Gluck *et al.* [40,41]. For the rho mesons, we have applied the same PDFs as for the pions as in Refs. [27,28]. This model for the pion and ρ self-energies has been earlier applied successfully in the intermediate-energy region and provides quite a solid description of a wide range of phenomenology in pion-, electron-, and photon-induced reactions in nuclei (see, e.g., Refs. [27,28,42–46]).

B. Target mass corrections

Target mass corrections have been incorporated by means of the approximate formula [30], which for $F_2^{\rm TMC}(x, Q^2)$ is

given by

$$F_2^{\rm TMC}(x, Q^2) \simeq \frac{x^2}{\xi^2\gamma^3} F_2(\xi, Q^2)\left[1 + \frac{6\mu x\xi}{\gamma}(1-\xi)^2\right], \tag{23}$$

and, for $F_3^{\rm TMC}(x, Q^2)$, it is given by

$$F_3^{\rm TMC}(x, Q^2) \simeq \frac{x}{\xi\gamma^2} F_3(\xi, Q^2)\left[1 - \frac{\mu x\xi}{\gamma}(1-\xi)\ln\xi\right], \tag{24}$$

where $\mu = \frac{M^2}{Q^2}$, $\gamma = (1 + \frac{4x^2M^2}{Q^2})^{1/2}$ and ξ is the Nachtmann variable defined as

$$\xi = \frac{2x}{1+\gamma}. \tag{25}$$

C. Coherent nuclear effects

For the shadowing and antishadowing nuclear effects we use the model developed by Kulagin and Petti in Ref. [12]. We quote their formulas here only for completeness. Following their notation, we have the ratios for the coherent nuclear correction to the structure functions F_T and F_3; namely, $\delta F_i^{\nu(\bar{\nu})A} = \delta R_i^{\nu(\bar{\nu})} F_i^{\nu(\bar{\nu})N}$ with $i = T, 2, 3$:

$$\delta R_T^{\nu(\bar{\nu})} = \delta R^{(0,+)} \pm \beta\delta R^{(1,-)} \frac{F_T^{(\nu-\bar{\nu})(1)}}{2F_T^{\nu(\bar{\nu})N}}, \tag{26}$$

$$\delta R_3^{\nu(\bar{\nu})} = \delta R^{(0,-)} \pm \beta\delta R^{(1,+)} \frac{F_3^{(\nu-\bar{\nu})(1)}}{2F_3^{\nu(\bar{\nu})N}} \pm (\delta R^{(0,+)} - \delta R^{(0,-)}) \frac{F_3^{(\nu-\bar{\nu})(s)}}{2F_3^{\nu(\bar{\nu})N}}. \tag{27}$$

In the above equations, the labels (I, C) with $I = 0, 1$ and $C = \pm$ stand for the classification in terms of isospin and C parity of the scattering states. The parameter $\beta = \frac{Z-N}{A}$ must be set equal to 0 if we are considering an isoscalar nucleus. Even for ^{56}Fe because we are considering it as an isoscalar nucleus. In the above equations, the plus (minus) sign refers to the neutrino (antineutrino). We assume the same correction factor for F_2 and F_T:

$$\delta F_2^{\nu(\bar{\nu})A} = \delta F_T^{\nu(\bar{\nu})A} = \delta R_T^{\nu(\bar{\nu})} F_T^{\nu(\bar{\nu})N} = \delta R_T^{\nu(\bar{\nu})} F_2^{\nu(\bar{\nu})N}. \tag{28}$$

IV. RESULTS AND DISCUSSION

In this section we present and discuss the results of our numerical calculations. In the local-density approximation, the

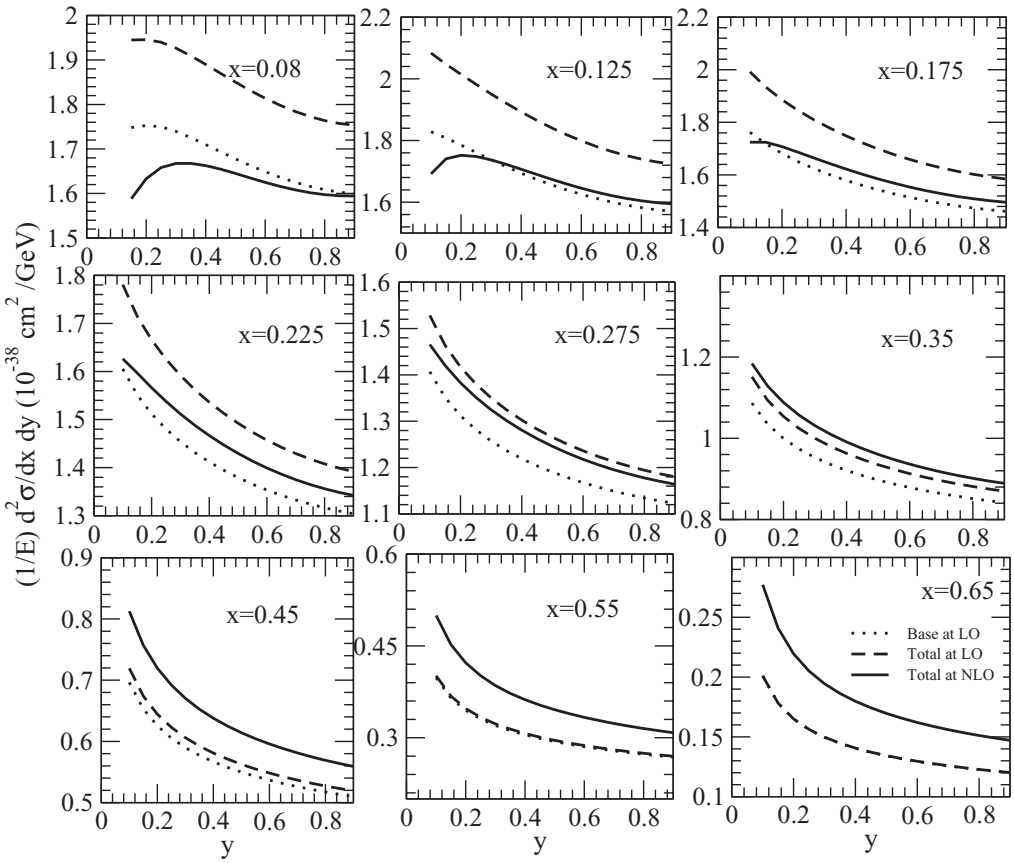

FIG. 12. $\frac{1}{E}\frac{d^2\sigma}{dxdy}$ vs y at different x for ν_μ-induced ($E_{\nu_\mu} = 60$ GeV) reaction in ^{12}C. Lines have the same meaning as in Fig. 2.

nuclear spectral functions depend on the nuclear density and, in the present calculations, we have used harmonic oscillator density for the ^{12}C nucleus and two-parameter Fermi density for the ^{56}Fe nucleus. The density parameters are taken from Ref. [47].

Using Eqs. (13) and (14), we have calculated the F_2^A and F_3^A structure functions in the iron nucleus with target mass correction and CTEQ6.6 parton distribution functions (PDFs) at LO [35]. We call this as our base (Base) result. Hereafter we include pion and rho cloud contributions in F_2^A and the shadowing corrections in F_2^A and F_3^A, which we call our full calculation (Total). In Figs. 2 and 3, we have shown these numerical results along with the experimental data of CDHSW [3] and NuTeV [9] for a wide range of x and Q^2. The effect of shadowing is about 3% to 5% at $x = 0.1$, $Q^2 = 1$ to 5 GeV^2 and 1% to 2% at $x = 0.2$, $Q^2 = 1$ to 5 GeV^2, which dies out with the increase in x and Q^2. In the case of F_2^A there are pion and rho cloud contributions. The pion contribution is very dominant in comparison to the rho contribution. The pion contribution is significant in the region of $0.1 < x < 0.4$. Thus, we find that the shadowing corrections seem to be negligible compared to the other nuclear effects. It is the meson cloud contribution which is dominant at low and intermediate x for F_2. In these figures we also show the results of our full calculation at NLO. We find that, in general, the results at NLO are in better agreement with the experimental observations; however, at some values of x and Q^2, LO results agree slightly better with data. This happens, for example, at $x = 0.65$. As discussed in Ref. [28], that region is affected by high-momentum components of the nucleon wave function and by possible off-shell effects that are not included in our approach. Thus, we should not draw any strong conclusion about this point. Furthermore, in Figs. 2 and 3, we have not included the additional uncertainty of ±2.1% that was mentioned as the normalization uncertainty in the NuTeV analysis. Moreover, the experimental results of CDHSW [3] and NuTeV [9] also differ among themselves. MINERνA [22] and other proposed experiments may be able to measure these structure functions with better precision.

Recently, we have studied the effect of nuclear medium on the electromagnetic nuclear structure function $F_2(x, Q^2)$ in nuclei using the same model as mentioned in Sec. III. We have obtained the ratio $R(x, Q^2) = \frac{2F_2^A}{AF_2^D}$ ($A = {}^9$Be, ^{12}C,^{40}Ca, ^{56}Fe) and compared our results [28] with the recent JLab results of Ref. [32] as well as with some of the older experiments [48]. The deuteron structure functions have been calculated using the same formulas as in Eqs. (13) and (14), but we perform the convolution with the deuteron wave function squared instead of the spectral function. See Ref. [31] for full details about the deuteron structure functions. We have used the parametrization

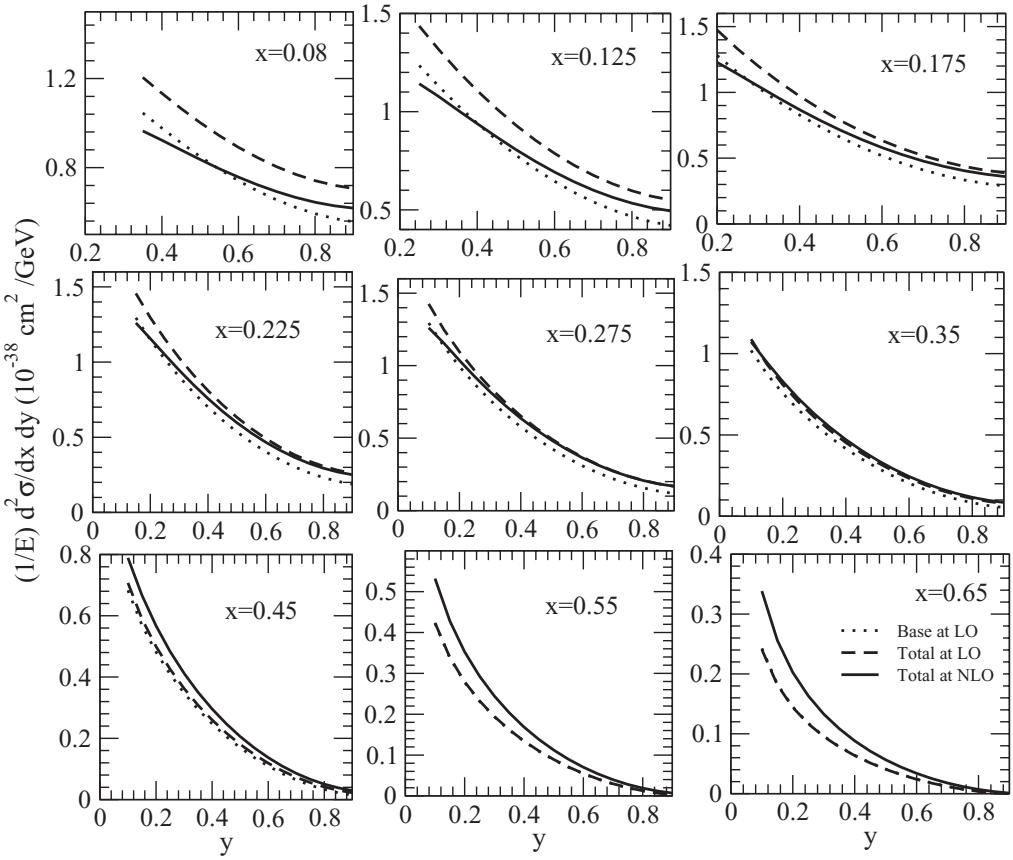

FIG. 13. $\frac{1}{E}\frac{d^2\sigma}{dxdy}$ vs y at different x for $\bar{\nu}_\mu$-induced ($E_{\bar{\nu}_\mu} = 20$ GeV) reaction in ^{12}C. Lines have the same meaning as in Fig. 2.

given in Ref. [49] for the deuteron wave function of the Paris N-N potential. We found that the results agree with those of JLab [32].

To understand this ratio in the weak sector we have studied the ratio of structure functions $R(x, Q^2) = \frac{2F_i^A}{AF_i^D}(i = 2, 3)$ in the neutrino and antineutrino induced deep inelastic scattering. This is important because there are several groups [14–21] who have phenomenologically studied the nuclear effects in parton distribution functions (PDFs). Aside from some minor differences, the main differences in their studies are the choice of the experimental data sets and the parametrization of the PDFs at the input level. In most of these studies the experimental data have been taken from the charged lepton nucleus ($l^{\pm}A$) scattering and the Drell-Yan (DY) data. A few of them also include neutrino scattering data (νA) in the parametrization of nuclear PDFs for the analysis of deep inelastic neutrino or antineutrino cross sections in nuclei. The reliability of the nuclear correction factor for the weak-interaction-induced processes obtained from the $l^{\pm}A + \mathrm{DY}$ data may be questioned, or how good would be the description if one also combines the νA data? Recently, Kovarik *et al*. [20] have phenomenologically studied the nuclear correction factor by taking two data sets (one $l^{\pm}A + \mathrm{DY}$ data set and the other set of νA data in iron from the NuTeV measurements) and observed that the nuclear effects are different, particularly at low and intermediate x. Here in the present work we have studied the nuclear effects in the ratio for $\frac{2F_i^A}{AF_i^D}(i = 2, 3)$ in iron at $Q^2 = 5$ GeV^2 and the results are shown in Figs. 4 and 5. Here, we have also shown the results obtained from the phenomenological studies of Tzanov *et al*. [9], Hirai *et al*. [15], Eskola *et al*. [18], and Schienbein *et al*. [21]. We find that our results for the ratio $R(x, Q^2) = \frac{2F_2^A}{AF_2^D}$ are similar to what we have obtained for the electromagnetic interaction [28], while the ratio $R(x, Q^2) = \frac{2F_3^A}{AF_3^D}$ is different in nature. It may be seen that the results of the different phenomenological studies differ between themselves as well as from our results. Whereas in most [9,15] of the phenomenological analyses the nuclear correction factor in F_2 and F_3 are taken to be the same, we are finding it to be different. Although the nuclear effects like Fermi motion and binding corrections are the same in F_2 and F_3 and have been incorporated by using a spectral function obtained for nuclear matter and implemented in nuclei using the local-density approximation, the differences in the results for F_2 and F_3 in our model are due to the fact that, in the F_2 structure function, there are meson cloud contributions whereas in F_3 this is absent, there is a different target mass correction, and a different kinematical factor as can be seen from Eqs. (13) and (14). We have observed that the effect of meson clouds is large at low and intermediate x. There

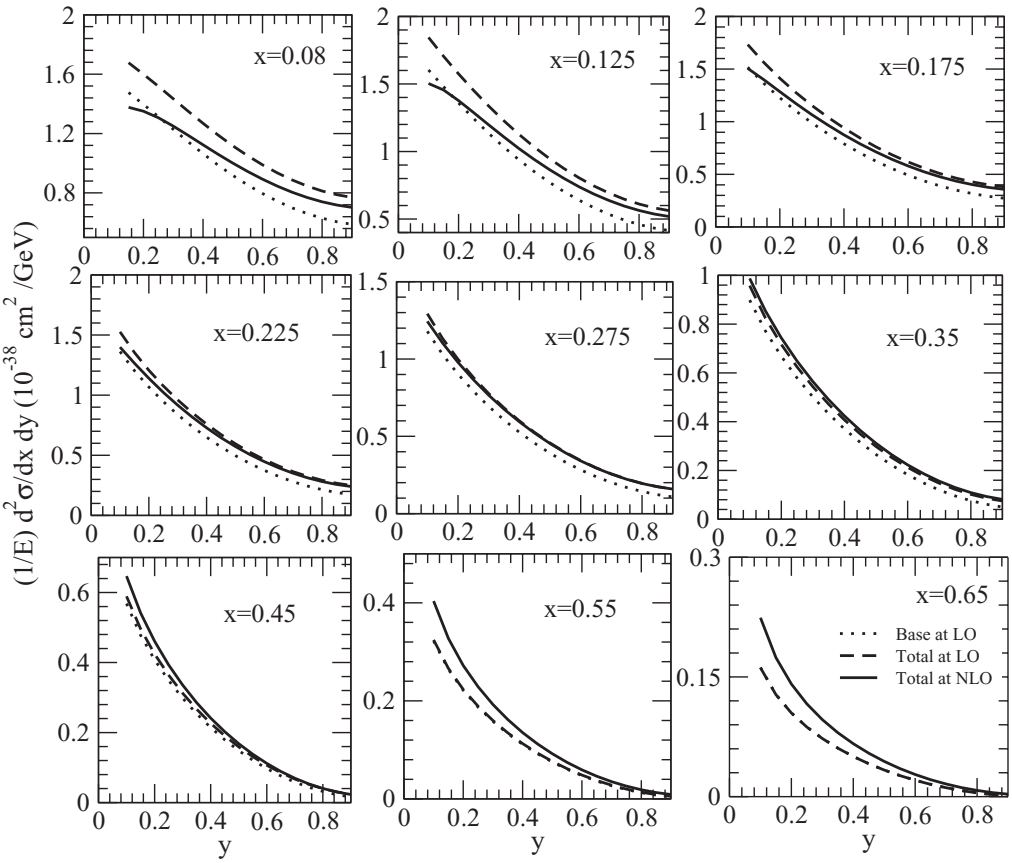

FIG. 14. $\frac{1}{E}\frac{d^2\sigma}{dxdy}$ vs y at different x for $\bar{\nu}_\mu$-induced ($E_{\bar{\nu}_\mu} = 60$ GeV) reaction in ^{12}C. Lines have the same meaning as in Fig. 2.

is an almost negligible shadowing correction. Therefore, we conclude that it is not appropriate to take the same correction factor for the F_2 and F_3 nuclear structure functions.

In Figs. 6 and 7, we show the results for $\frac{1}{E}\frac{d^2\sigma}{dxdy}$ in ^{56}Fe at $E_{\nu_\mu} = 65$ and 150 GeV, respectively. The calculations for the double differential cross sections have been performed for $Q^2 > 1$ GeV^2. Similarly, in Figs. 8 and 9, we show the results for $\frac{1}{E}\frac{d^2\sigma}{dxdy}$ induced by antineutrinos in ^{56}Fe at $E_{\bar{\nu}_\mu} = 65$ and 150 GeV, respectively. We find that the results of the full calculations at NLO are, in general, in good agreement with the experimental observations of the CDHSW [3] and NuTeV [9] collaborations.

In the present model, for the pion and rho mesons contributions, the expressions for which are given in Eqs. (16) and (22), respectively, the expression includes pion and rho meson self-energies [27], which earlier have been quite successfully used in the calculations of pion-, electron-, and photon-induced reactions in nuclei. It has some uncertainties such as the specific form of the spin-isospin interaction, specially for the ρ meson. To understand the effect of the variation in the parameters of the pion and rho meson self-energies Λ and Λ_ρ, respectively, on the differential scattering cross section we plot $\frac{1}{E}\frac{d^2\sigma}{dxdy}$ in Fig. 10 by taking Λ, $\Lambda_\rho = 0.8$, 1.0, and 1.2 GeV. We find that a 20% variation in the values of Λ, results in a change of 4% to 6% in the cross section at low x, which decreases to 2% to 3% around $x = 0.4$ to 0.5, and after that it dies out. To observe the effect of nonisoscalarity, we also studied (not shown) isoscalarity vs nonisoscalarity corrections and found that the nonisoscalar correction is around 2% to 3%.

Figures 11 and 12 are the results for $\frac{1}{E}\frac{d^2\sigma}{dxdy}$ in ^{12}C induced by neutrinos at $E_{\nu_\mu} = 20$ and 60 GeV, respectively, and Figs. 13 and 14 are the corresponding results in ^{12}C induced by antineutrinos. The results in carbon will be useful in the analysis of data by the NOMAD [25] Collaboration as well as of the proposed NuSOnG experiment [23,24]. The NOMAD [50] experiment is primarily meant to measure the neutrino and antineutrino cross sections with better precision and to constrain the nuclear models. Therefore, our study of the nuclear-medium effects would be a good test when the data will be available.

V. CONCLUSIONS

To summarize our results, we have studied nuclear effects in the structure functions $F_2^A(x, Q^2)$ and $F_3^A(x, Q^2)$ in carbon and iron nuclei using a many-body theory to describe the spectral function of the nucleon in the nuclear medium for all Q^2. The local-density approximation has been used to apply the results for the finite nuclei. The use of the spectral function is to incorporate Fermi motion and binding effects. We have used CTEQ [35] PDFs in the numerical evaluation. Target mass correction (TMC) has been considered. We have taken the effects of mesonic degrees of freedom, shadowing, and antishadowing in the calculation of F_2^A and shadowing and antishadowing effects in the calculation of F_3^A. We have found that the mesonic cloud (basically pion) gives an important contribution to the cross section. These numerical results have been compared with the experimental observations of the CDHSW [3] and NuTeV [9] collaborations. Using these structure functions we obtained differential scattering cross sections for iron and carbon nuclei and compared the results for iron from the experimentally observed values obtained by the CDHSW [3] and NuTeV [9] collaborations. We also find that the effect of the nuclear medium is also quite important even for deep inelastic scattering, and the ratio of the structure functions in nuclei to deuteron or free nucleon is different in $F_2^A(x, Q^2)$ and $F_3^A(x, Q^2)$.

ACKNOWLEDGMENTS

This research was supported by DGI and FEDER funds, under contracts FIS2008-01143/FIS, FIS2006-03438, and the Spanish Consolider-Ingenio 2010 Program CPAN (CSD2007-00042), by Generalitat Valenciana contract PROMETEO/2009/0090 and by the EU HadronPhysics2 project, Grant Agreement No. 227431. I.R.S. acknowledges support from the Ministerio de Educacion. M.S.A. wishes to acknowledge the financial support from the University of Valencia and the Aligarh Muslim University under the academic exchange program and also to the DST, Government of India for financial support under Grant SR/S2/HEP-0001/2008. H.H. acknowledges the Maulana Azad National Program.

[1] J. J. Aubert *et al.*, Phys. Lett. B **105**, 322 (1981); **123**, 275 (1983).
[2] D. Allasia *et al.*, Z. Phys. C **28**, 321 (1991).
[3] J. P. Berge *et al.*, Z. Phys. C **49**, 187 (1987).
[4] K. Varvell *et al.* Z. Phys. C **36**, 1 (1991).
[5] E. Oltman *et al.*, Z. Phys. C **53**, 51 (1992).
[6] W. G. Seligman *et al.*, Phys. Rev. Lett. **79**, 1213 (1997).
[7] A. V. Sidorov *et al.*, Eur. Phys. J. C **10**, 405 (1999).
[8] Bonnie T. Fleming *et al.*, Phys. Rev. Lett. **86**, 5430 (2001).
[9] M. Tzanov *et al.*, Phys. Rev. D **74**, 012008 (2006).
[10] *Proc. of the 12th International Workshop on Superbeams, Neutrino Factories, and Beta Beams (NuFact-2010)*, AIP Conf. Proc. (2011).
[11] *Seventh International Workshop on Neutrino-Nucleus Interactions in the Few-GeV Region*, [http://nuint11.in/].
[12] S. A. Kulagin and R. Petti, Phys. Rev. D **76**, 094023 (2007).
[13] M. Sajjad Athar, S. K. Singh, and M. J. Vicente Vacas, Phys. Lett. B **668**, 133 (2008).
[14] M. Hirai, S. Kumano, and T. H. Nagai, Phys. Rev. C **70**, 044905 (2004); Phys. Rev. D **64**, 034003 (2001).
[15] M. Hirai, S. Kumano, and T. H. Nagai, Phys. Rev. C **76**, 065207 (2007).
[16] K. J. Eskola, H. Paukkunen, and C. A. Salgado, JHEP 07 (**2008**) 102.
[17] A. Bodek and U. K. Yang, Nucl. Phys. B, Proc. Suppl. **112**, 70 (2002).

[18] K. J. Eskola, V. J. Kolhinen, and C. A. Salgado, Eur. Phys. J. C **9**, 61 (1999).
[19] K. Kovarik, AIP Conf. Proc. **1382**, 158 (2011).
[20] K. Kovarik *et al*., Phys. Rev. Lett. **106**, 122301 (2011).
[21] I. Schienbein, J. Y. Yu, K. Kovarik, C. Keppel, J. G. Morfin, F. I. Olness, and J. F. Owens, Phys. Rev. D **80**, 094004 (2009).
[22] David Schmitz, *Status of the MINERA Neutrino Scattering Experiment at Fermilab, NuInt11* [http://nuint11.in/]; MINERvA Collaboration, B. Eberly, AIP Conf. Proc. **1222**, 253 (2010).
[23] Michael H. Shaevitz, Journal of Physics: Conference Series **136**, 022025 (2008).
[24] NuSOnG Collaboration, T. Adams *et al*., Int. J. Mod. Phys. A **24**, 671 (2009).
[25] R. Petti (private communication).
[26] P. Fernandez de Cordoba and E. Oset, Phys. Rev. C **46**, 1697 (1992).
[27] E. Marco, E. Oset, and P. Fernandez de Cordoba, Nucl. Phys. A **611**, 484 (1996).
[28] M. Sajjad Athar, I. Ruiz Simo, and M. J. Vicente Vacas, Nucl. Phys. A **857**, 29 (2011).
[29] C. Garcia-Recio, J. Nieves, and E. Oset, Phys. Rev. C **51**, 237 (1995).
[30] I. Schienbein *et al*., J. Phys. G **35**, 053101 (2008).
[31] S. A. Kulagin and R. Petti, Nucl. Phys. A **765**, 126 (2006).
[32] J. Seely *et al*., Phys. Rev. Lett. **103**, 202301 (2009).
[33] P. Fernandez de Cordoba, E. Marco, H. Muther, E. Oset, and Amand Faessler, Nucl. Phys. A **611**, 514 (1996).
[34] C. G. Callan Jr. and D. J. Gross, Phys. Rev. Lett. **22**, 156 (1969).
[35] Pavel M. Nadolsky *et al*., Phys. Rev. D **78**, 013004 (2008); [http://hep.pa.msu.edu/cteq/public].
[36] J. A. M. Vermaseren *et al*., Nucl. Phys. B **724**, 3 (2005).
[37] S. Moch, J. A. M. Vermaseren, and A. Vogt, Nucl. Phys. B **813**, 220 (2009).
[38] W. L. van Neerven and A. Vogt, Nucl. Phys. B **568**, 263 (2000); **588**, 345 (2000).
[39] C. Itzykson and J. B. Zuber, *Quantum Field Theory* (McGraw-Hill, New York, 1980).
[40] M. Gluck, E. Reya, and A. Vogt, Z. Phys. C **53**, 651 (1992).
[41] M. Gluck, E. Reya, and I. Schienbein, Eur. Phys. J. C **10**, 313 (1999).
[42] E. Oset, H. Toki, and W. Weise, Phys. Rep. **83**, 281 (1982).
[43] R. C. Carrasco and E. Oset, Nucl. Phys. A **536**, 445 (1992).
[44] J. Nieves, E. Oset, and C. Garcia-Recio, Nucl. Phys. A **554**, 554 (1993).
[45] J. Nieves, E. Oset, and C. Garcia-Recio, Nucl. Phys. A **554**, 509 (1993).
[46] A. Gil, J. Nieves, and E. Oset, Nucl. Phys. A **627**, 543 (1997).
[47] H. de Vries, C. W. de Jager, and C. de Vries, At. Data Nucl. Data Tables **36**, 583 (1971).
[48] J. Gomez *et al*., Phys. Rev. D **49**, 4348 (1994).
[49] M. Lacombe, B. Loiseau, R. Vinh Mau, J. Cote, P. Pires, and R. de Tourreil, Phys. Lett. B **101**, 139 (1981).
[50] J. Altegoer *et al*., Nucl. Instrum. Methods Phys. Res. A **404**, 96 (1998).